Typeset with jjap2.cls <ver.1.0> **Regular Paper**

Viscoelasticity evolution in protein layers during binding reactions evaluated using high-frequency wireless and electrodeless quartz crystal microbalance biosensor without dissipation

Tomohiro Shagawa, Hiroomi Torii, Fumihito Kato, Hirotsugu Ogi*, and Masahiko Hirao

Graduate School of Engineering Science, Osaka University, Toyonaka, Osaka 560-8531, Japan

In this study, we demonstrate the effectiveness of a resonance acoustic microbalance with a naked embedded quartz (RAMNE-Q) biosensor for evaluating viscoelastic property changes in thin protein layers during protein deposition reactions without dissipation measurement. Quartz crystal microbalance (QCM) biosensors have conventionally been adopted for the viscoelasticity evaluation of adsorbed protein layers by measuring dissipation as well as resonance frequency. However, dissipation, or the vibrational energy loss, is easily affected by many factors and is rarely measured with sufficiently high accuracy. To evaluate viscoelasticity only from a reliable frequency response, one needs to perform an ultrahigh-frequency measurement, which is here achieved using the RAMNE-Q biosensor. Simultaneous frequency measurement is performed for fundamental and overtone modes up to 406 MHz of a 58 MHz RAMNE-Q biosensor during various binding reactions, and evolutions of viscosity, shear modulus, and thickness of adsorbed protein layers are inversely evaluated. A marked difference is observed in the viscosity evolution between specific and nonspecific binding reactions. Furthermore, the reversed frequency response appears, which indicates the modification of the protein structure into a rigid structure.

1. Introduction

The quartz crystal microbalance (QCM) biosensor is a mass-sensitive biosensor.[1–3] It detects adsorbed mass through the resonance-frequency shift of the quartz resonator when target proteins are captured on the receptor-immobilized quartz surface. It is a label-free biosensor and allows one to perform more reliable and simplified assays. Furthermore, a QCM biosensor can achieve real-time monitoring of binding reactions to yield the binding affinity. The wireless-electrodeless approach for the quartz-crystal resonator improved its sensitivity significantly[4] and allowed its integration into optical microscopy.[5,6] Thus, it is a powerful tool for studying interactions among biomolecules.

QCM biosensors have recently been utilized for the evaluation of the viscoelastic properties of protein layers by measuring dissipation as well as resonance frequencies: this is known as the QCM-D technique.[7–9] In the conventional QCM-D method, an AT-cut quartz crystal with a fundamental resonance frequency near 5 MHz, corresponding to the crystal thickness of about 170 μm, is used. The method requires the measurement of dissipation to evaluate viscoelasticity, but dissipation, representing the vibrational energy loss, is sensitive not only to protein viscoelasticity but also more markedly

*E-mail: ogi@me.es.osaka-u.ac.jp

to many other factors, including the changes in solution viscosity, solution flow rate, and the holding condition of the resonator. In particular, the mechanical contacts when clamping the resonator tightly significantly increase the apparent dissipation, and this energy loss is much larger than the intrinsic dissipation in the viscoelastic protein layer, making it difficult to evaluate changes in the viscoelastic properties in a thin protein layer accurately. Even a minute pressure change caused by switching the solution or by flow-rate fluctuation owing to the difference in solution viscosity affects the clamping condition, which can change the dissipation value more significantly than the change in the viscoelasticity in the protein layer. The accurate measurement of dissipation in a resonator system is never straightforward when the resonator system has mechanical contacts to the outside.[10)]

A favorable way of evaluating protein viscoelasticity is to utilize only frequency changes, which can be measured with higher accuracy and reliability than dissipation, but this requires extremely high frequency measurements: The viscoelastic properties of the protein layer cause a discrepancy from the mass-loading effect (Sauerbrey equation) at higher overtones because the soft layer fails to respond to the fast surface movement. However, this effect is never marked for a low-frequency QCM, because the acoustic shear field extends into the solution area owing to the solution viscosity and its decay length is inversely proportional to the square root of frequency. For a 5 MHz QCM, for example, it is about 250 nm from the surface, which is much larger than the protein layer thickness in many assays and little deformation occurs in such a thin layer. A high-frequency QCM is thus important for determining viscoelastic properties without measuring ambiguous dissipation.

We previously developed a resonance acoustic microbalance with a naked embedded quartz (RAMNE-Q) by a MEMS process,[11–14)] where both surfaces and all sides of an electrodeless naked quartz resonator can be used. The naked quartz crystal is supported without any fixed parts, and it is embedded in a microchannel fabricated in a Si wafer by sandwiching between two glass wafers. The RAMNE-Q biosensor provides a solution to the problem that the highly sensitive QCM biosensor, the quartz oscillator that is much thinner than those in conventional QCMs, is fragile and breaks easily during its installation in the sensor cell. We have recently used a RAMNE-Q biosensor to evaluate protein viscoelasticity with frequencies up to 174 MHz.[15)] In that study, however, we were able to determine only the layer thickness and viscosity, assuming a constant shear modulus, because only two modes were monitored. Higher frequencies are needed for evaluating the shear modulus and viscosity simultaneously.

In this study, we propose the viscoelasticity measurement of a thin protein layer with the high-frequency RAMNE-Q biosensor using frequencies over 400 MHz, the highest frequency in this field of study. Using a three-layer model,[16–18)] we inversely evaluated the evolutions of thickness, viscosity, and shear modulus of a growing protein layer from the frequency changes without using dissipation. We clearly confirm the difference in viscoelasticity between the protein layers formed by specific and nonspecific bindings. Also, we find that the reversed frequency change occurs in some cases. The amount of frequency change is normally largest for the fundamental mode, but this ordinary behavior

changes in some protein layers. We also find that a distinguishing viscosity evolution causes such a reversed frequency behavior.

2. Inverse calculation model

Figure 1(a) shows the three-layer model, which consists of the Newtonian fluid layer for flowing solution, the Voigt viscoelastic layer for proteins involving the solution, and the elastic quartz layer. Solving the wave equations with the boundary conditions of the stress-free states at the bottom and top surfaces and assuming the continuities of the shear stress and particle velocity under the nonslip condition at each interface, the shift of the nth overtone resonance frequency from its free vibration, Δf_n, is given by

$$\Delta f_n \approx \frac{1}{2\pi\rho_q h_q}\mathrm{Im}\left(\kappa_p\xi_p\frac{1-Ae^{2\xi_p h_p}}{1+Ae^{2\xi_p h_p}}\right), \tag{1}$$

where

$$A = \frac{\kappa_p\xi_p + \eta_s\xi_s\tanh(\xi_s h_s)}{\kappa_p\xi_p - \eta_s\xi_s\tanh(\xi_s h_s)}, \kappa_p = \frac{\mu_p^*}{j\omega_n},$$

$$\xi_p = \sqrt{-\rho_p\omega_n^2/\mu_p^*}, \xi_s = \sqrt{j\rho_s\omega_n/\eta_s}, \mu_p^* = \mu_p + j\omega_n\eta_p.$$

Here, h, ρ, μ, η, and ω_n represent the thickness, mass density, shear modulus, viscosity, and angular frequency of the nth mode, respectively. The subscripts q, p, and s denote quantities in the quartz, protein, and solution layers, respectively. Because ρ_q, μ_q, ρ_s, and η_s are known, Δf_n becomes a function of h_p, η_p, μ_p, ρ_p, and n. We, however, find that the mass density of the protein layer is insensitive to resonance frequency in comparison with the other parameters, as shown in Fig. 1(b). We, therefore, assume ρ_p to be that of water (ρ_p = 1000 kg/m^3) to reduce the ambiguity of the parameters and evaluate the other three parameters inversely from four frequency responses by the least-squares method. Furthermore, conventional assays lead to the formation of multiple protein layers, and the viscoelastic properties dynamically change during the formation of protein layers, making the evaluation of the viscoelasticity of individual layers complicated and unrealistic because of many ambiguous parameters. We then evaluate the macroscopic viscoelasticity of protein layers by assuming multiple protein layers as a single protein layer.

In this model, the protein layer is regarded as a uniform viscoelastic material, but it actually consists of adsorbed protein molecules and liquid at their interspaces. Because the apparent viscosity of the protein layer represents the loss of oscillation energy, it should be sensitive to the binding condition of protein molecules. In a specific binding system, protein molecules are tightly captured on the surface, and the apparent viscosity in this layer will be equivalent to that of the liquid in this layer. On the other hand, proteins are weakly adsorbed in a nonspecific binding system and move with a phase lag, showing higher apparent viscosity, as indicated in a previous study.[15)]

3. Experimental procedure

The RAMNE-Q biosensor shown in Fig. 2 was used. A 58 MHz AT-cut quartz resonator of 28.5 μm thickness was packaged in the rectangular space of the Si microchannel by the anodic bonding method. The quartz plate was lightly supported by 10-μ-diameter Si and glass micropillars. The quartz plate was washed with piranha solution (98% H_2SO_4: 33% H_2O_2 =7:3) for 30 min, rinsed with ultrapure water, and cleaned using a UV-ozone cleaner. It was then installed in the sensor cell. The two flat antennas set outside the microchannel generated and detected the shear vibration of the quartz wirelessly during solution flow. Figure 3 shows resonance spectra of the fundamental mode and up to 7th overtone measured in a phosphate-buffered saline (PBS) solution flow at a flow rate of 200 μl/min. The quality factor (Q factor) improves at overtones because of the smaller acoustic-shear length in the solution (it becomes 28 nm at the 7th mode). These spectra show asymmetric shapes, which are caused by the coexistence of spurious modes. (We actually observed some spurious modes in a slightly higher frequency region of the main resonance frequency.) The spurious modes could contribute to the broadening and asymmetry of resonant peaks, depending on their vibrational strength in the solution.[19)]

In this study, four measurements were performed. First, a streptococcal protein G (SPG) solution (200 μg/ml in a PBS solution) was injected to immobilize the SPG molecules nonspecifically on the quartz surfaces, and then a human immunoglobulin G (IgG) solution (100 ng/ml in PBS) was injected to cause the specific binding reaction between SPG and IgG. SPG specifically binds with various IgG molecules with high affinity[20,21)] through its C-terminal domains.[22)] With this experiment, we investigate the difference in viscoelasticity change between specific and nonspecificic binding assays.

Second, to confirm the viscoelastic properties estimated in the first experiment, we investigated the viscoelasticity evolution for a different binding system, that between staphylococcus aureus protein A (SPA) and rabbit IgG (rIgG), with a similar protein-layer thickness. SPA captures IgG molecules with high binding affinity, acting as the IgG receptor.[23,24)] We nonspecifically immobilized SPA molecules on the quartz surfaces by immersing the crystal in the SPA solution (200 μg/ml SPA in PBS) for 16 h, and it was set in the sensor cell. The rIgG solution (1000 ng/ml in PBS) was then injected.

Third, we investigated the effect of a multistep injection on the overall viscoelasticity. After the nonspecific immobilization of the SPA molecules (200 μg/ml in PBS) on the quart surfaces, the anti-rIgG antibody (ArIgG) solution (10 μg/ml in PBS) was injected. This unusually caused the reversed frequency response. The rIgG solutions of 100 and 1000 ng/ml were then injected to generate the multi-protein layers.

Lastly, we confirmed the reversed frequency response system between SPA and rIgG. The SPA molecules were immobilized in ultrapure water and the rIgG solution (1 μg/ml in ultrapure water) was injected. Our previous study revealed that ultrapure water significantly enhances the nonspecific immobilization of SPA on the naked quartz surface,[11)] and thus we expect that a large number of rIgG molecules will be captured in this assay.

SPG was purchased from Cell Sciences (Product No. CRP154B), hIgG from Athens Research &

Technology (Product No. 16-16-090707), SPA and rIgG from Invitrogen (Products Nos. 10-1100 and 02-6102, respectively), and ArIgG from Arista Biologicals (Product No. ABGAR-0500). All other chemical substances were purchased from Wako Pure Chemical Industries, Ltd.

4. Results

Figures 4(a) and 4(b) show the measured frequency responses with solid lines for injections of the SPG and hIgG solutions. Figure 4(c) shows those during the injection of rIgG solution on the SPA immobilized quartz chip. In these experiments, the amount of frequency change is restricted to the frequency increase, which is the usual frequency behavior often observed in previous QCM-D experiments.[8,9] The corresponding evolutions of the protein-layer viscoelastic parameters are shown in Figs. 4(d)–4(f) (changes in the evaluated parameters were smoothed for ease of comprehension). The reconstructed frequency changes are shown in Figs. 4(a)–4(c) with dashed lines. Their good agreement with the experimental results support the reliability of the deduced parameters.

Figure 5(a) shows the frequency changes for the injection of the anti-rIgG antibody on the SPA immobilized quartz surfaces. Importantly, the frequency change does not follow the usual rule. Instead, the 3rd and 5th overtone modes decrease more significantly than the fundamental mode. The deduced viscoelastic parameters for this assay are shown in Figs. 5(d)–5(f) with black lines. Despite the monotonic thickness increase, the viscosity first increases and then decreases. The increase in the shear modulus is markedly significant. Figures 5(b) and 5(c) show frequency changes for subsequent injections of 100 and 1000 ng/ml rIgG solutions, respectively. In these cases, the frequency-decrement order becomes normal. Their corresponding evolutions of viscoelastic parameters are shown in Figs. 5(d)–5(f). Figure 5(g) shows the reconstructed frequency responses when a 5 MHz QCM is used for injections of rIgG solutions. In this case, almost no separation is observed in frequency responses, indicating that we would fail to determine the viscoelasticity when using the low-frequency QCM.

Figure 6(a) shows the frequency response for the injection of rIgG on SPA immobilized quartz surfaces with the running buffer of ultrapure water. The unusual frequency response is clearly observed: The amount of frequency change is largest for the 5th mode, and that of the fundamental mode is smallest. The protein-layer parameters are shown in Figs. 6(b)–6(d), where the viscosity increases and then decreases despite continuous increases in the thickness and stiffness. Figure 6(e) shows the estimated frequency changes in the case of a 5 MHz QCM, where again no frequency separation occurs, indicating the difficulty in evaluating the viscoelasticity with such a low-frequency QCM.

5. Discussion

The RAMNE-Q biosensor system developed here detects the frequency change of each mode simultaneously regardless of whether deposition is nonspecific or specific. However, responses in the higher modes are clearly different between them, as shown in Figs. 4(a) and 4(b). The first three modes (f_1, f_3, and f_5) show identical behavior in the case of the nonspecific binding of SPG on the quartz surfaces [Fig. 4(a)], whereas the frequencies of the three overtones are separated from that of the fundamental

mode in the specific binding reaction between SPG and hIgG [Figs. 4(b)]. (Our previous biosensors using frequencies up to 174 MHz[15] should fail to determine the viscosity from data in Fig. 4(a), because no separation occurs between the 58 and 174 MHz modes.) During the binding of SPG on quartz, the viscosity decreases and the stiffness increases markedly. The viscosity reached is, however, fairly higher than that of water despite the large amount of water present in the protein layer. This suggests that the nonspecifically adsorbed SPG molecules are flexible and move with a phase lag responding to the quartz surface, showing larger energy loss. The subsequent specific binding by SPG and hIgG further decreases the viscosity and increases the stiffness, making the protein layer more rigid through the formation of truss-like structures of IgG molecules, as indicated in a previous study.[15] This trend is also seen in the other binding system between SPA and rIgG, as shown in Figs. 4(c)–4(f). We obtained the identical amount of frequency change in this system to Fig. 4(b) by changing the concentration of rIgG. The resultant viscoelastic parameters [blue lines in Fig. 4(c)] reached values close to those in the binding system between SPG and hIgG. Thus, the viscoelasticity is reproducible even with different receptors when the total thickness is identical, and this confirms the reliability of the measurement and analysis proposed in this study.

Very importantly, we clearly observed the reversed frequency response in Fig. 5(a), and this is well reproduced as shown by the dashed lines, with the evolutions of the protein-layer parameters in Figs. 5(d)–5(f). The notable trend is the nonmonotonic viscosity change despite monotonic increases in thickness and stiffness. This suggests the reconstruction of the protein layer. Because a large number of rIgG molecules are adsorbed on the receptor layer, some of them bind with a nonspecific matter, which increases the viscosity temporarily [Fig. 7(a)]. As the deposition rate decreases with time, such weakly adsorbed molecules will find more specific binding sites to reconstruct a more rigid protein layer, causing a viscosity decrease [Fig. 7(b)]. The subsequent injections of the rIgG antigen, however, cause the typical order of frequency changes, meaning that no marked modification occurs in the base antibody layer during the deposition of the rIgG; the stiffness and viscosity remain nearly unchanged, although the last injection of a higher-concentration antigen solution increases the viscosity, suggesting that overloaded molecules are nonspecifically adsorbed.[15]

The reversed frequency response was confirmed in another assay experiment as shown in Fig. 6(a), where ultrapure water was used as the running buffer. We previously showed that many SPA molecules are adsorbed with ultrapure water rather than PBS solution,[11] capturing a large number of IgG molecules. As shown in Figs. 6(b)–6(d), similar evolutions of the protein-layer parameters to those shown in Figs. 5(d)–5(f) are obtained: the viscosity first increases and then decreases, while the stiffness and thickness increase monotonically. Thus, the modification of the protein layer will proceed during the binding reaction of IgG molecules, as illustrated in Fig. 7.

We note that the above important results would not be obtained with low-frequency QCMs. Figures 5(g) and 6(e) show frequency changes for a 5 MHz QCM reconstructed with the obtained viscoelasticity evolutions, where frequencies were negligibly separated, making the determination of the

viscoelastic parameters unrealistic. Thus, the high-frequency QCM is the key to the inverse evaluation of the viscoelasticity of protein layers from only frequency.

6. Conclusions

Using the RAMNE-Q biosensor with a fundamental resonance frequency of 58 MHz, we measured frequency changes of the fundamental and three overtone modes, which exceeded 400 MHz, during a series of binding reactions. The evolutions of the thickness, viscosity, and shear modulus of the protein layer were determined from the frequency changes without measuring dissipation. Although a conventional 5 MHz QCM will fail to show separation in the frequency responses, the high-frequency QCM achieves the evaluation of viscoelastic properties without measuring dissipation. We reveal that the protein layer becomes stiffer and less viscous, forming a rigid structure, and that the frequency reversed phenomenon appears during the structural modification when many molecules are captured. We furthermore demonstrated that the three-layer model is principally applicable, even to adsorption on a thick multilayer. These results indicate the effectiveness of RAMNE-Q biosensors as a new technique for evaluating viscoelastic properties.

Acknowledgement

This study was supported by the Funding Program for Next Generation World-Leading Researchers by the Cabinet Office, Government of Japan.

References

1) G. Sauerbrey, Z. Phys. **155**,206 (1959) [in German].
2) H. Muramatsu, M. Dicks, E. Tamiya, and I. Karube, Anal. Chem. **59**, 2760 (1987).
3) Y. Liu, X. Yu, R. Zhao, D. Shangguan, Z. Bo, and G. Liu, Biosens. Bioelectron. **19**, 9 (2003).
4) H. Ogi, K. Motohisa, K. Hatanaka, T. Ohmori, M. Hirao, and M. Nishiyama, Biosens. Bioelectron. **22**, 3238 (2007).
5) H. Hamada, H. Ogi, K. Noi, H. Yagi, Y. Goto, and M. Hirao, Jpn. J. Appl. Phys. **54**, 07HE01 (2015).
6) H. Ogi, M. Fukushima, H. Hamada, K. Noi, M. Hirao, H. Yagi, and Y. Goto, Sci. Rep. **4**, 6960 (2014).
7) F. Höök, B. Kasemo, T. Nylander, C. Fant, K. Sott, and H. Elwing, Anal. Chem. **73**, 5796 (2001).
8) A. Patel, K. Kanazawa, and C. W. Frank, Anal. Chem. **81**,6021 (2009).
9) M. Yan, C. Liu, D. Wang, J. Ni, and J. Chang, Langmuir **27**, 9860 (2011).
10) H. Ogi, M. Hirao, and T. Honda, J. Acoust. Soc. Am. **98**, 458 (1995).
11) F. Kato, H. Ogi, T. Yanagida, S. Nishikawa, M. Nishiyama, and M. Hirao, Jpn. J. Appl. Phys. **50**, 07HD03 (2011).
12) F. Kato, H. Ogi, T. Yanagida, S. Nishikawa, M. Hirao, and M. Nishiyama, Biosens. Bioelectron. **33**, 139 (2012).
13) F. Kato, K. Tsurimoto, H. Ogi, and M. Hirao, Jpn. J. Appl. Phys. **52**, 07HD11 (2013).
14) H. Ogi, Proc. Jpn. Acad. Ser. B **89**, 401 (2013).
15) T. Shagawa, H. Torii, F. Kato, H. Ogi, and M. Hirao, Jpn. J. Appl. Phys. **54**, 068001 (2015).
16) C. Reed, K. Kanazawa, and J. H. Kaufman, J. Appl. Phys. **68**, 1993 (1990).
17) M. V. Voinova, M. Jonson, and B. Kasemo: J. Phys.: Condens. Matter. **9**, 7799 (1997).
18) M. V. Voinova, M. Rodahl, M. Jonson, and B. Kasemo, Phys. Scr. **59**, 391 (1999).
19) T. Yamaguchi, S. Miyake, and S. Koda, J. Phys. Chem. **114** 8126 (2010).
20) B. Akerström and L. Björck, J. Biol. Chem. **261**, 10240 (1986).
21) U. Sjöbring, L. Björck, and W. Kastern, J. Biol. Chem. **266**, 399 (1991).
22) L. Björck and W. Kastern, J. Immunol. **133**, 969 (1984).
23) E. O'Keefe and V. Bennett, J. Biol. Chem. **25**, 561 (1980).
24) D. C. Hanson and V. N. Schumaker, J. Immunol. **132**, 1397 (1984).

Figure Captions

Fig. 1. (Color online) (a) Three-layer model composed of AT quartz layer, Voigt viscoelastic protein layer, and Newtonian solution layer. (b) Dependences of the resonance-frequency change on the four parameters in the protein layer, determined using a 58 MHz QCM: (b-1)–(b-4) show dependences on thickness, viscosity, shear modulus, and mass density, respectively. Black, red, blue, and green lines represent Δf_1, $\Delta f_3/3$, $\Delta f_5/5$, and $\Delta f_7/7$, respectively.

Fig. 2. (Color online) (a) Schematic of the RAMNE-Q chip biosensor and (b) the cross-sectional view along A-A'.

Fig. 3. Resonant spectra of the RAMNE-Q biosensor with fundamental resonance frequency of 58 MHz measured during PBS flow. The quality-factor (Q-factor) values are shown.

Fig. 4. (Color online) Frequency responses and parameter evolutions of protein layer. Measured (solid lines) and reconstructed (broken lines) frequency responses during injections of (a) SPG (200 μg/ml in PBS) on naked quartz surfaces, (b) hIgG (100 ng/ml in PBS) on the SPG-immobilized surfaces, and (c) rIgG (1000 ng/ml in PBS) on the SPA-immobilized surfaces. In these figures, black, red, blue, and green lines represent Δf_1, $\Delta f_3/3$, $\Delta f_5/5$, and $\Delta f_7/7$, respectively. Corresponding evolutions of (d) thickness, (e) viscosity, and (f) stiffness for individual injections are shown.

Fig. 5. (Color online) Measured (solid lines) and reconstructed (broken lines) frequency responses during injections of (a) ArIgG (10 μg/ml in PBS) on the SPA-immobilized quartz surfaces, (b) rIgG (100 ng/ml), and (c) rIgG (1000 ng/ml) on the SPA-immobilized quartz surfaces, and corresponding evolutions of (d) thickness, (e) viscosity, and (f) shear modulus. (g) Reconstructed frequency responses for 5 MHz QCM with the parameters in (d)–(f). In (a)–(c), and (g), black, red, blue, and green lines represent Δf_1, $\Delta f_3/3$, $\Delta f_5/5$, and $\Delta f_7/7$, respectively.

Fig. 6. (Color online) (a) Measured (solid lines) and reconstructed (broken lines) frequency responses during the injection of rIgG (1 μg/ml in ultrapure water) on the SPA-immobilized quartz chip, and corresponding evolutions of (b) thickness, (c) viscosity, and (d) shear modulus. (e) Reconstructed frequency responses for 5 MHz QCM with the parameters in (b)–(d). In (a) and (e), black, red, blue, and green lines represent Δf_1, $\Delta f_3/3$, $\Delta f_5/5$, and $\Delta f_7/7$, respectively.

Fig. 7. (Color online) Schematics of dynamic modification of protein structures on the quartz surface. (a) Many IgG molecules are captured in a short time and some of them show nonspecific binding that increases the viscosity. (b) Formation of rigid protein layer owing to transition of IgG binding from nonspecific binding to specific binding, which leads to the decrease in the viscosity.

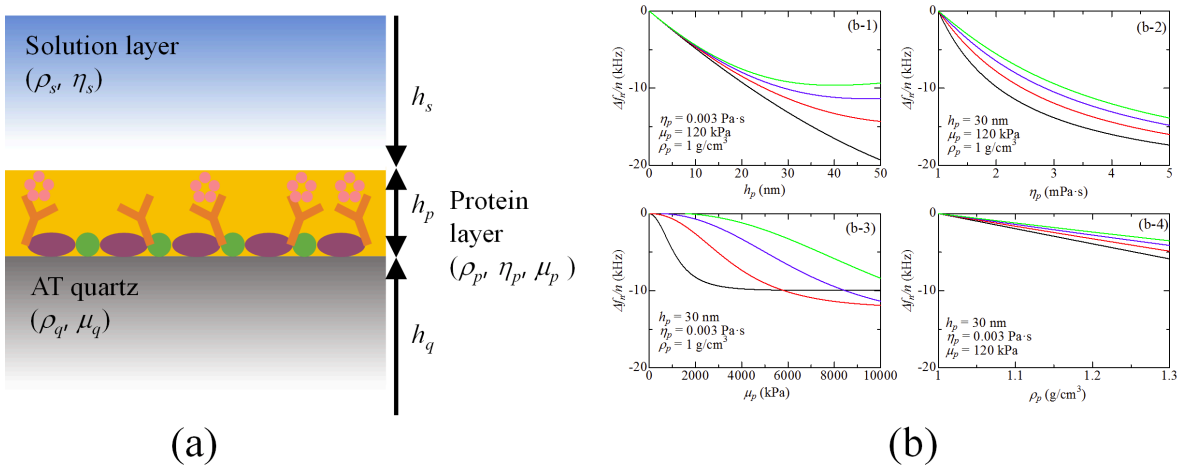
Solution layer
(ρ_s, η_s)
h_s
h_p
Protein layer
(ρ_p, η_p, μ_p)
AT quartz
(ρ_q, μ_q)
h_q
(a)
(b-1)
η_p = 0.003 Pa·s
μ_p = 120 kPa
ρ_p = 1 g/cm^3
h_p (nm)
(b-2)
h_p = 30 nm
μ_p = 120 kPa
ρ_p = 1 g/cm^3
η_p (mPa·s)
(b-3)
h_p = 30 nm
η_p = 0.003 Pa·s
ρ_p = 1 g/cm^3
μ_p (kPa)
(b-4)
h_p = 30 nm
η_p = 0.003 Pa·s
μ_p = 120 kPa
ρ_p (g/cm^3)
$\Delta f_n/n$ (kHz)
(b)

Fig. 1.

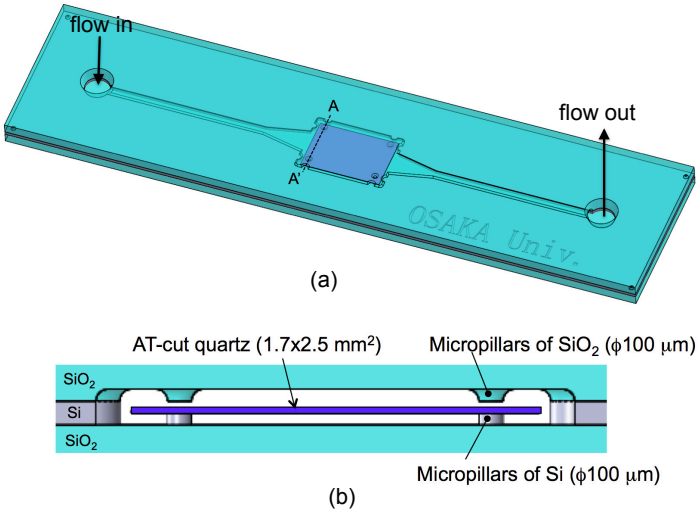
flow in
A
A'
flow out
OSAKA Univ.
(a)
AT-cut quartz (1.7x2.5 mm²)
Micropillars of SiO₂ (ϕ100 μm)
SiO₂
Si
SiO₂
Micropillars of Si (ϕ100 μm)
(b)

Fig. 2.

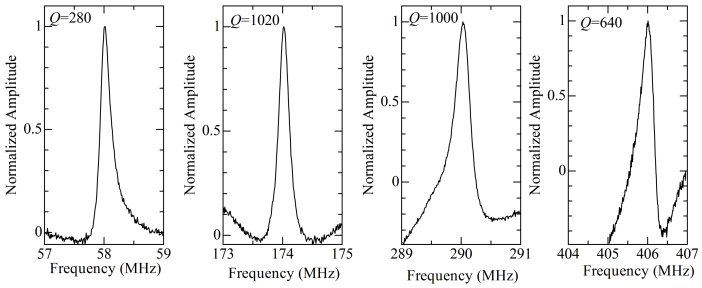
Q=280
Q=1020
Q=1000
Q=640
Normalized Amplitude
Frequency (MHz)
57
58
59
173
174
175
289
290
291
404
405
406
407
0
0.5
1

Fig. 3.

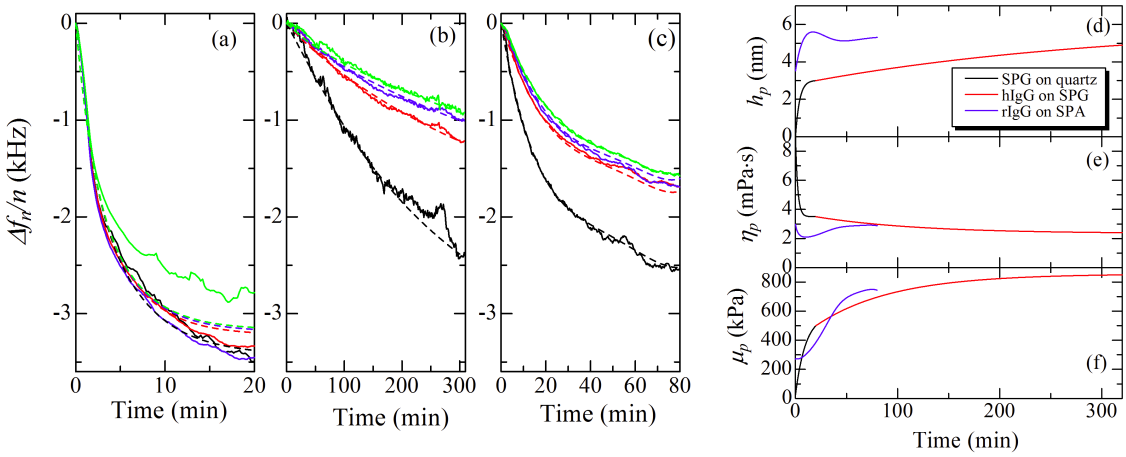
(a)
(b)
(c)
(d)
(e)
(f)
$\Delta f_n/n$ (kHz)
Time (min)
h_p (nm)
η_p (mPa·s)
μ_p (kPa)
SPG on quartz
hIgG on SPG
rIgG on SPA

Fig. 4.

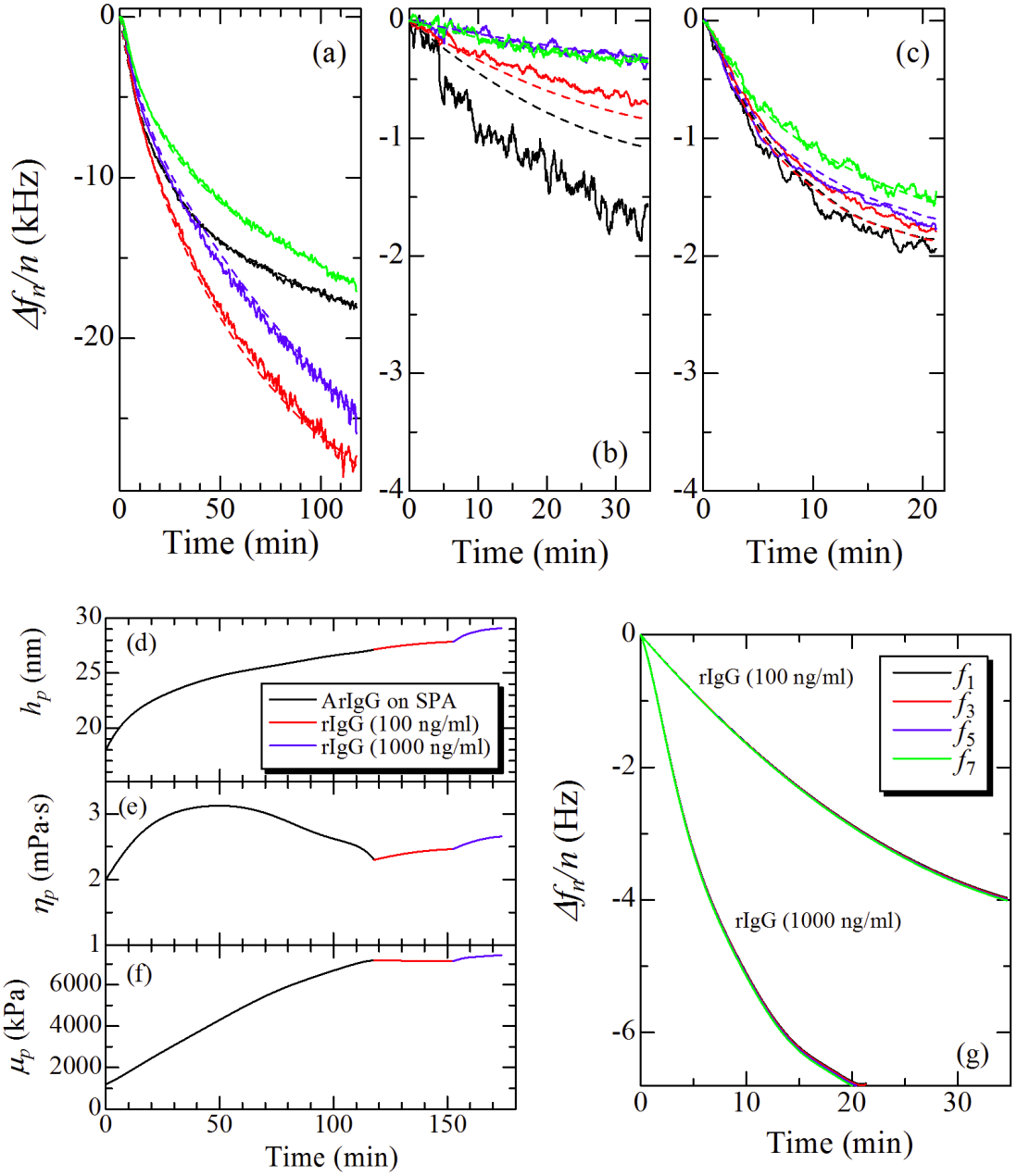
(a)
(b)
(c)
(d)
(e)
(f)
(g)
$\Delta f_n/n$ (kHz)
Time (min)
h_p (nm)
η_p (mPa·s)
μ_p (kPa)
ArIgG on SPA
rIgG (100 ng/ml)
rIgG (1000 ng/ml)
$\Delta f_n/n$ (Hz)
f_1
f_3
f_5
f_7

Fig. 5.

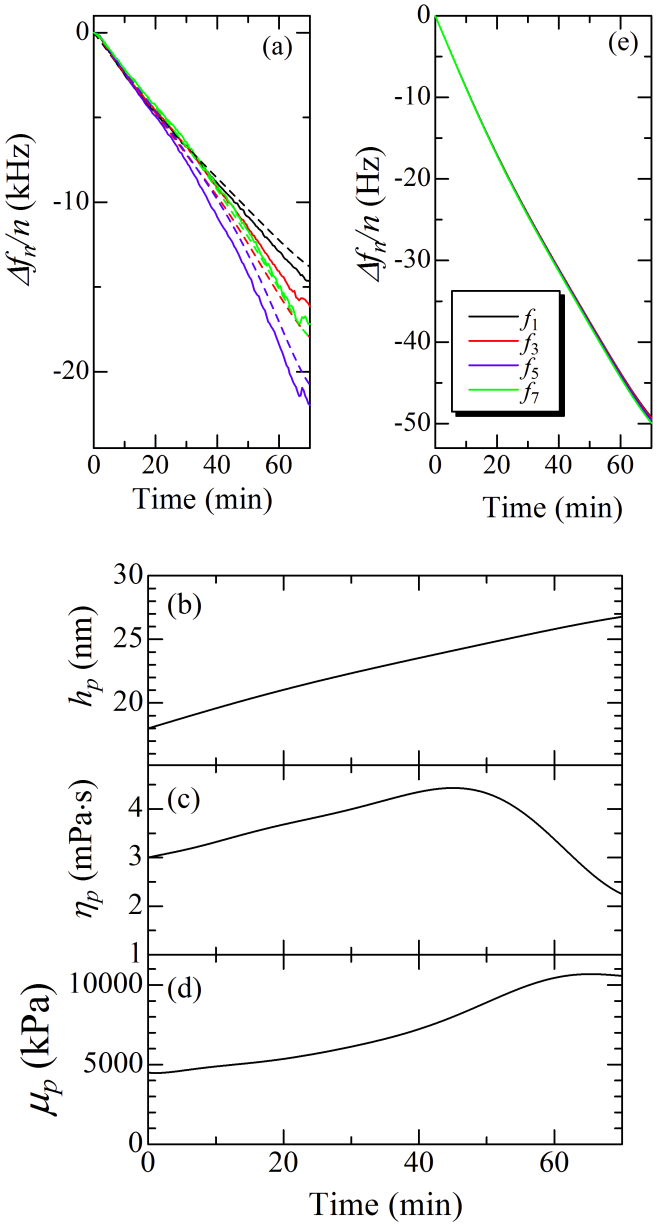
(a)
(e)
(b)
(c)
(d)
$\Delta f_n/n$ (kHz)
$\Delta f_n/n$ (Hz)
h_p (nm)
η_p (mPa·s)
μ_p (kPa)
Time (min)
f_1
f_3
f_5
f_7

Fig. 6.

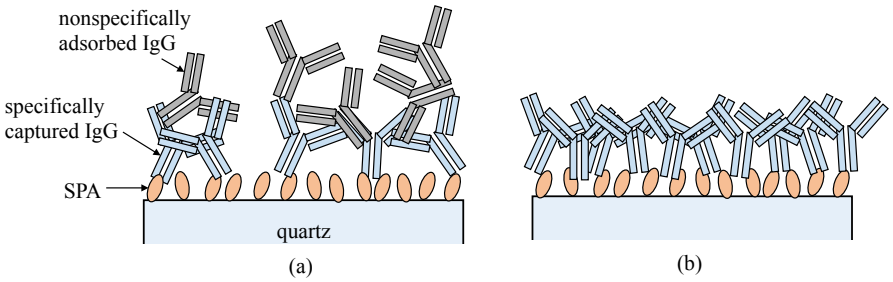
nonspecifically
adsorbed IgG
specifically
captured IgG
SPA
quartz
(a)
(b)

Fig. 7.